Block Coordinate Descent Based Algorithm for Image Reconstruction in Photoacoustic Tomography

Anjali Gupta, Ashok Kumar Kajla and Ramesh Chandra Bansal

Abstract Photoacoustic (PA) imaging is a rising, congenital, in vivo biomedical imaging configuration combining equally optics and ultrasonics used for tumor angiogenesis monitoring. A nanosecond laser pulse is accustomed to illuminate biological tissue at a light wavelength typically in the near-infrared (NIR) window when deep light entrance into tissue is desired. The emission pressure rise at the origin is reciprocal to the immersed power and the force wave drives within smooth organic tissues as an audible wave also recognized as Photoacoustic wave. Several photoacoustic image reconstruction algorithms have been developed which includes analytic methods in terms of filtered back-projection (FBP) rather algorithms founded on Fourier transform but these methods generally give suboptimal images. In this paper, we developed an algorithm based on block coordinate descent method for image reconstruction in photoacoustic tomography (PAT). Block coordinate descent (BCD) algorithms optimize the target function over individual segment, at every sub-repetition, whereas keeping all the other segments fixed. This scheme is used to compute pseudoinverse of system matrix and reconstruct image for pressure distribution in photoacoustic tomography. The proposed BCD method is compared with back-projection (BP) method, direct regularized pseudoinverse computation and conjugate gradient based method using simulated phantom data sets.

Keywords Photoacoustic tomography · Reconstruction algorithms · Linear image reconstruction · Block coordinate descent algorithm

A. Gupta (✉) · A. K. Kajla · R. C. Bansal
Department of Electronics and Communication Engineering, Arya Institute of Engineering and Technology, Jaipur, India
e-mail: guptaanjali1803@gmail.com

A. K. Kajla
e-mail: kajla_ashok@yahoo.com

R. C. Bansal
e-mail: dr_rcbansal@yahoo.co.in

A. Gupta · A. K. Kajla · R. C. Bansal
RTU, Kota, India

A. K. Luhach et al. (eds.), *Smart Computational Strategies: Theoretical and Practical Aspects*, https://doi.org/10.1007/978-981-13-6295-8_8

1 Introduction

The area of photoacoustic tomography has proficient significant expansion in recent years. Even though various immaculate optical imaging configurations, containing two-photon microscopy, confocal microscopy, and optical coherence tomography have been extremely prosperous, none of these techniques can supply insight over $\sim$1 mm into dispersion organic tissues, consequently they are premised on quasi-ballistic and ballistic photons. Hence there has been a invalid in high-resolution optical imaging over this penetration limit [1, 2]. Photoacoustic tomography, that merges superior ultrasonic resolution and persistent optical oppose in a single modality, has damaged throughout this restriction and filled this faulty.

The region of photoacoustic tomography (PAT) has developed an excellent deal in recent years. PAT is an imaging technology premised on the photoacoustic result. PAT merges strong optical contrast and high ultrasonic resolution in a single configuration, competent of supplying high-resolution functional, structural, and molecular imaging in vivo in optically spreading organic tissue at new nadir. PAT includes ultrasonic detection, optical irradiation, and image structure. The tissue is normally illuminated by a short-pulsed laser beam to generate thermal and audio impulse responses. Regionally immersed light is transformed into heat, that is in addition transformed to a pressure increase via thermoelastic enlargement of the tissue. The beginning pressure rise resolute by the local optical energy displacement also known by specific optical absorption in the unit of J/m^3 and another mechanical and thermal characteristics spread in the tissue as an ultrasonic wave, that is mentioned to as a photoacoustic wave. The photoacoustic wave is discovered by ultrasonic transducers established external the tissue, generating electric signals. The electric signals are then digitized, magnified, and shifted to a computer, where an image is created.

PAT relies on some absorbed photons, moreover scattered or unscattered, to generate photoacoustic signals as long as the photon excitation is serene thermally [3].

Figure 1 shows a schematic scheme to illustrate the photoacoustic effect, where a short duration pulse is an incident on the photoacoustic source and subsequently the incidental light is immersed and transformed into acoustic signals via thermal growth. PAT is extremely sensitive to optical preoccupation. PAT deals on murky context when no absorption endures, the background signal is nothing. Similar dark background allows touchy discovery. In the existence of absorption, the foreground signal is proportionate to the absorption factor. Some little partial alter in optical absorption factor interprets into an equal quantity of fractional alter in PAT signal, that means a relative sensitivity of 100% [4]. The spatial resolution is acquired from ultrasonic identification in the photoacoustic emission phase. Ultrasonic dispersion is much slighter than optical dispersion. The wavelength of the discovered photoacoustic wave is adequately little. As consequence, photoacoustic waves supply superior resolution than optical waves over the smooth depth restrict. Among other factors, the bandwidth and the center frequency of the ultrasonic discovery system

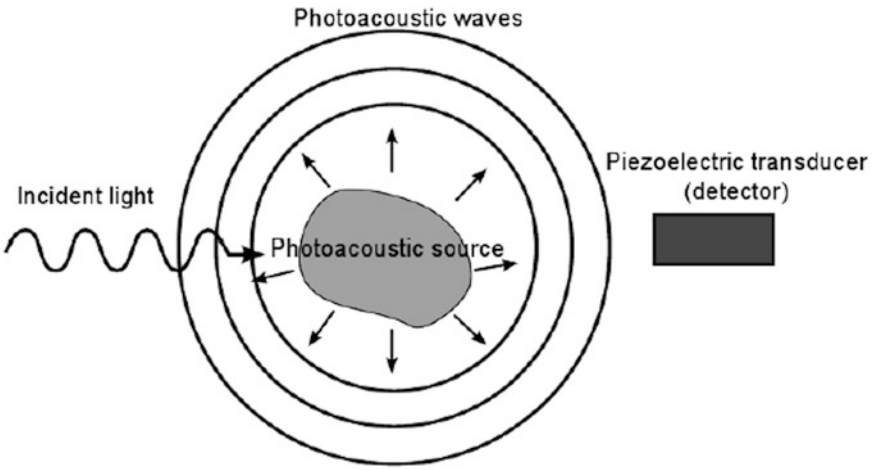

Fig. 1 Fundamental rule of the photoacoustic consequence. Incident light is immersed and transformed into acoustic waves by thermal extension. The acoustic waves are discovered by a piezoelectric transducer [1]

mainly establish the spatial resolution of PAT [5]. The higher the center frequency and the wider the bandwidth, the superior the spatial resolution is.

2 Problem in Photoacoustic Tomography

Photoacoustic imaging primarily deals with two problems, forward and inverse problems. The forward problem involves solving the photoacoustic wave differential equation for a given medium. The inverse problem involves solving for the initial pressure of the medium from the available surface level measurements

(a) Forward Problem

$$\left(\nabla^2 - \frac{1}{v_s^2}\frac{\partial^2}{\partial t^2}\right)p(r,t) = -\frac{\beta}{k v_s^2}\frac{\partial^2 T(r,t)}{\partial t^2}, \tag{1}$$

where, $K = \frac{c_p}{\rho v_s^2 c_v}$ is the isothermal compressibility, ρ is the density of mass, c_v and c_p denotes the particular heat capacities at persistent volume and pressure, v_s implies the speed of sound ($\sim$1480 m/s in water), β denotes the thermal factor of volume increase, p and T denotes the change in pressure (in Pa) and temperature (in K), individually. $p(r,t)$ is the acoustic force at location r and time t.

In the above equation, the left-hand side explains the pressure wave expansion. The source name is described on the right side. The most normally utilized

numerical approaches for solving part differential equations in audios are finite-dissimilarity, finite-element, and boundary-element methods [6, 7]. Even though fine for various applications, for time-domain modeling of wideband or high-frequency waves, they can turn into awkward and slow. This is because of the requirement of various grid points per wavelength and little time-steps to diminish undesirable numerical dispersion. The pseudo-spectral technique that expresses a growth of the finite difference procedure can support decrease the first of these issues and the *k*-space way can assist to defeat the second.

(b) Inverse Problem

The inverse problem describes estimating the initial pressure distribution using the surface level measurements. One well-known method to solve the inverse problem is to make use of the system matrix which represents the system completely. The system which describes the PA signal acquisition procedure can be expressed by a Toeplitz matrix of a time-changing causal system. An image (dimension $n \times n$) gets reshaped into a large vector by arranging all the columns, represented by x, note that the dimensions of the image is $n^2 \times 1$. This implies the system matrix (A) contains dimensions of $m \times n^2$. Every column of A mentions the system's output to a corresponding entry in x. In here, the system's response is collected utilizing the *k*-wave pseudo-spectral technique. In other words, the pth column entry of A corresponds to the system's measured response to an impulse at the pth entry of x, i.e., $x(p) = 1$, while rest of the entries are zero. Note that the system response is time-varying, the columns of data are also arranged to result in a large vector having dimensions $m \times 1$. This system matrix (A) will be considered for the reconstruction methods which will be discussed in the following section. An illustration of how the system matrix (A) is being built is given in Fig. 2.

3 Image Reconstruction Methods in Photoacoustic Imaging

The forward model equation of photoacoustic imaging can be represented in form of matrix equation as

$$Ax = b \tag{2}$$

Here A represents a system matrix. The size of A in our study is 30,000 × 40,401. The image to be reconstructed is represented by the vector x. Vector x has the length of 40,401. The measurement vector is represented by b. It has a length of 30,000.

There are several ways to solve Eq. 2 but in essence, these methods can be classified as non-iterative and iterative methods. The following subsections introduce the methods used in this work to solve Eq. 2.

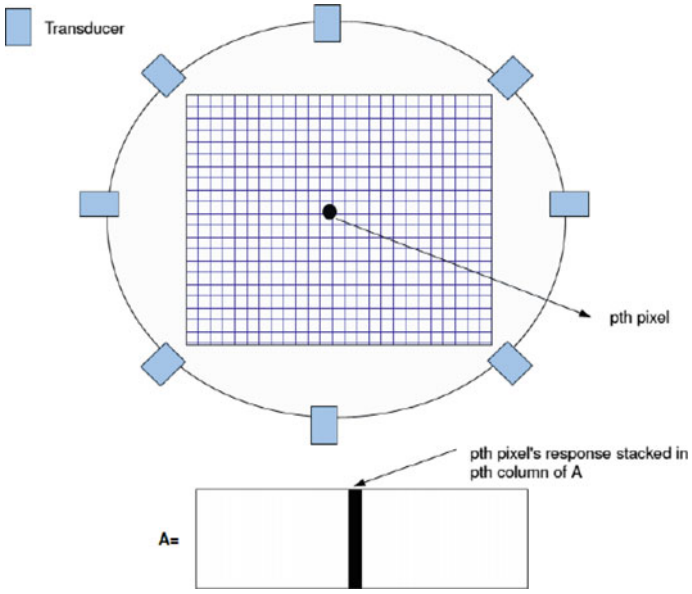

Fig. 2 An illustration of how the system matrix (A) is being built using the forward model which uses the pseudo-spectral method

(a) *Back-Projection (BP) Method*

The back-projection is the simplest image reconstruction scheme where the expression to compute the solution is given by [8],

$$x = A^{\mathrm{T}} b \tag{3}$$

Here, A^{T} is the transpose of system matrix A. Multiplication of A^{T} with measurement vector b is equivalent to back-projection. The back-projection method is computationally very efficient since it is a non-iterative method. Back-projection methods are t be the right choice for quantitative imaging. Moreover, the measurement vector, b is generally corrupted by noise, so this type of back-projection over-amplifies the noise.

(b) *Conjugate Gradient Method*

Conjugate gradient technique is a process to find the numerical solution of a system of linear equations. This conjugate gradient technique is often employed as an iterative procedure. For the system of equations given in 2, this iterative algorithm can be expressed in the following steps [9]:

The residual is given as

$$r_k = b - Ax_k \tag{4}$$

The basis vectors p can be written as,

$$p_k = r_k - \sum_{i<k} \frac{p_i^{\mathrm{T}} A r_k}{p_i^{\mathrm{T}} A p_i} p_i \tag{5}$$

$$\alpha_k = \frac{p_k^{\mathrm{T}} b}{p_k^{\mathrm{T}} A p_k}$$

The iterative solution for the Eq. 2 is given by the following equation:

$$x_{k+1} = x_k + \alpha_k p_k \tag{6}$$

This iterative equation is used to reconstruct the image which is represented by the vector x.

(c) *Regularized Pseudoinverse Computation Based Method*

For the least square problem of Eq. 2, the best fit solution is given as

$$x = A^+ b, \tag{7}$$

where A^+ is known as pseudoinverse of A. A^+ is given as

$$A^+ = \left(A^{\mathrm{T}} A\right)^{-1} A^{\mathrm{T}} \tag{8}$$

Hence the solution becomes,

$$x = \left(A^{\mathrm{T}} A\right)^{-1} A^{\mathrm{T}} b \tag{9}$$

This method is computationally quite expensive. Computation of A^+ requires a lot of time. Also, the solution x in Eq. 6 can be noisy. To improve the solution we use a regularization parameter λ such that the regularized pseudoinverse becomes

$$A_{\mathrm{reg}}^+ = \left(A^{\mathrm{T}} A + \lambda 1\right)^{-1} A^+ \tag{10}$$

And,

$$x = A_{\mathrm{reg}}^+ b \tag{11}$$

This equation is used to reconstruct the image which is represented by the vector x.

(d) *Block Coordinate Descent Method*

Block coordinate descent (BCD) technique implements the objective function on one segment (bunch of variables) x_j at every sub-iteration, while all the other segments $x_j \neq x_j$ are kept fixed. The universal convergence of the BCD iterates is established for minimizing a convex non-differentiable equation with definite separability and regularity characteristics [10].

In the case of the linear regression problem [11],

$$f(x) = \frac{1}{2}||b-Ax||^2 \tag{12}$$

If we minimize above equation over x_j with all x_j fixed such that $i \neq j$,

$$0 = \nabla_i f(x) = A_i^{\mathrm{T}}(Ax - b) = A_i^{\mathrm{T}}(A_i x_i + A_{-i}x_{-i} - b)$$

i.e., we get,

$$x_i = \frac{A_i^{\mathrm{T}}(b - A_{-i}x_{-i})}{A_i^{\mathrm{T}}A_i} \tag{13}$$

The iterative scheme in Eq. 13 is used to estimate the vector x.

Another approach is to first establish the blockwise pseudoinverse matrix using Eq. 13, i.e.,

$$A_i^{+} = \left(A_i^{\mathrm{T}}A_i\right)^{-1}A_i^{\mathrm{T}}$$

Hence,

$$x_i = A_i^{+}(b - A_{-i}x_{-i}) \tag{14}$$

Further, with use of regularization parameter λ, Eq. 14 can be rewritten as follows:

$$x_i = \left(A_i^{\mathrm{T}}A_i + \lambda I\right)^{-1}(b - A_{-i}x_{-i}) \tag{15}$$

In this study, the Eq. 15 is used for the reconstruction of the image represented by a vector x.

4 Results and Discussions

This section presents the details of the numerical experimental data used in the proposed method, LSQR-based method and other traditional methods used for comparison. In this study, three numerical phantoms were considered, a PAT phantom, a Derenzo phantom, and a blood vessel phantom. For all the results presented here the regularization parameter was set to =0.018 as this was the best-suited value observed for all imaging structures.

(a) *Numerical Blood Vessel Phantom*

Because of the large intrinsic contrast that blood cells give, photoacoustic imaging is broadly utilized for visualizing internal blood vessel formation, both in the brain and also under the skin. Figure 3a represents a blood vessel network utilized as numerical phantoms. The *k*-wave was utilized to produce the simulated PA result for 60 detector circular locations. 40 dB of noise was included in the simulated data. Figure 3 shows the reconstructions obtained through back-projection method, reconstruction obtained through blockwise computation of pseudoinverse and through direct pseudo inverse computation method.

(b) *Derenzo Numerical Phantom*

Derenzo phantom consists of many circular shapes of different size. This can be considered similar to tumors present under the skin. Figure 4 a shows a Derenzo phantom which has been used in the present study. The *k*-wave was utilized to produce the simulated PA data for 60 detector circular locations. 40 dB of noise was included in the simulated data. Figure 4 shows the reconstructions obtained through back-projection method, reconstruction obtained through blockwise computation of pseudoinverse and through direct pseudo inverse computation method.

(c) *PAT Numerical Phantom*

Figure 5 a shows a numerical PAT phantom image. The *k*-wave was utilized to produce the simulated PA data for 60 detector circular locations. Again, 40 dB of noise was included in the simulated data. Figure 5 represents the reconstructions obtained employing back-projection method, reconstruction obtained through blockwise computation of pseudoinverse and through direct pseudo inverse computation method.

Details of Computation Time

One of the important advantages of using BCD method to compute blockwise pseudoinverse for image reconstruction problem is because of its computational efficiency. BCD scheme for pseudoinverse calculation is much faster than direct pseudoinverse calculation using Eq. 10. We have used four blocks BCD methods for pseudoinverse calculation.

The experiments were performed on 128 GB RAM, Z820 hp machine. The following table compares the pseudoinverse computation time (Table 1).

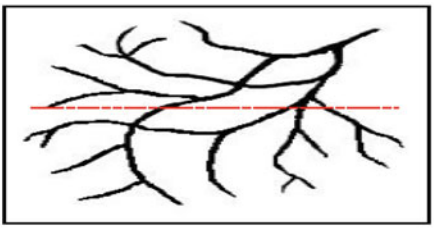

(a) Target

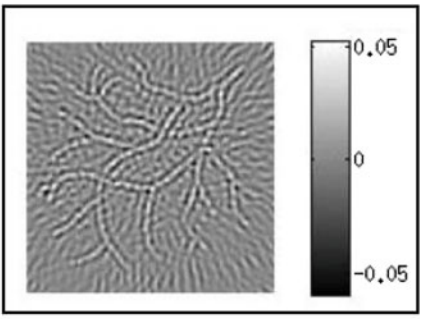

(b) Back Projection

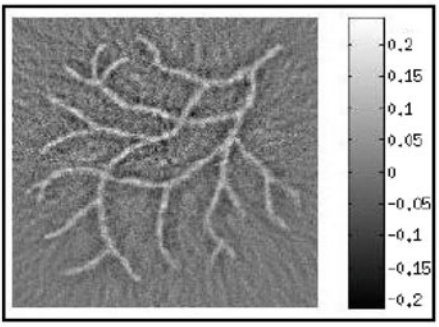

(C) BCD Reconstruction Scheme

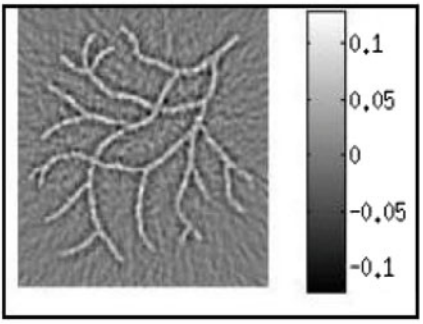

(d) Direct regularized Pseudo-inverse Computation

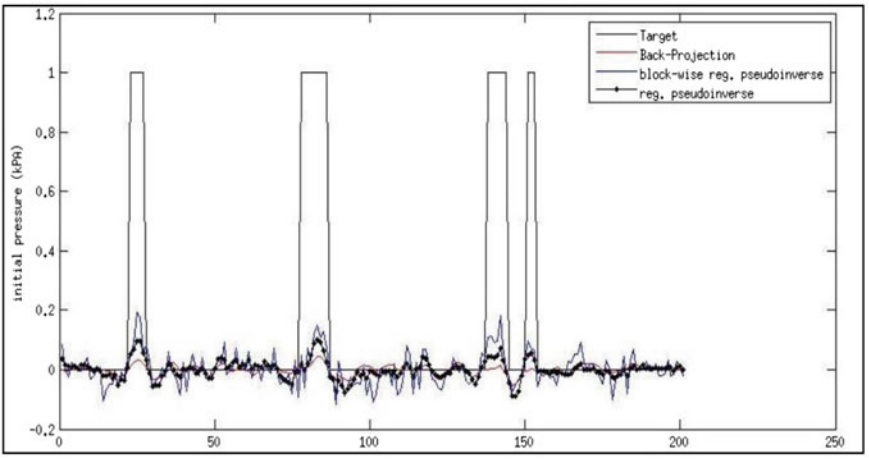

(e) Line profile for the dashed line along the target image

Fig. 3 Reconstructed photoacoustic image of a numerical blood vessel structure phantom as an imaging domain with an initial pressure rise of 1 kPa. **a** Target image, **b** back-projection (BP) reconstruction, **c** BCD scheme reconstruction, **d** reconstruction using regularized direct pseudo inverse computation and finally **e** the graph represents the line profile for the dashed line along the target image

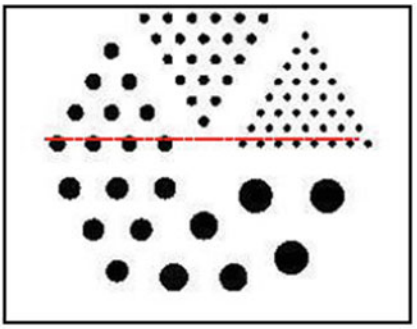

(a)Target

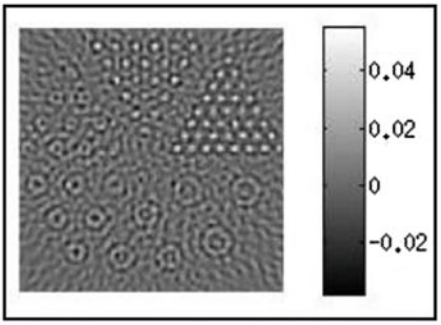

(b) Back Projection

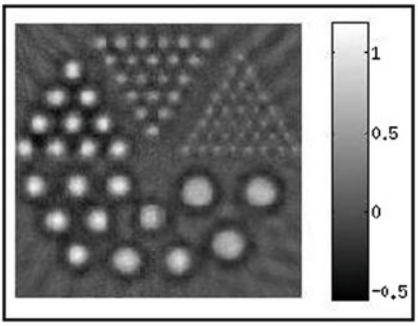

(c) BCD reconstruction scheme

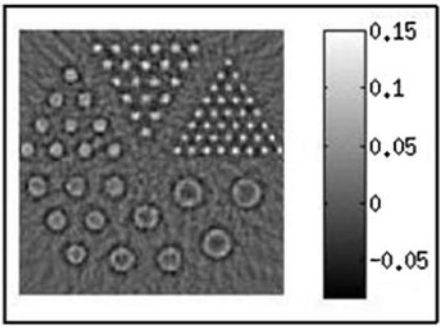

(d) Direct regularized Pseudo-inverse Computation

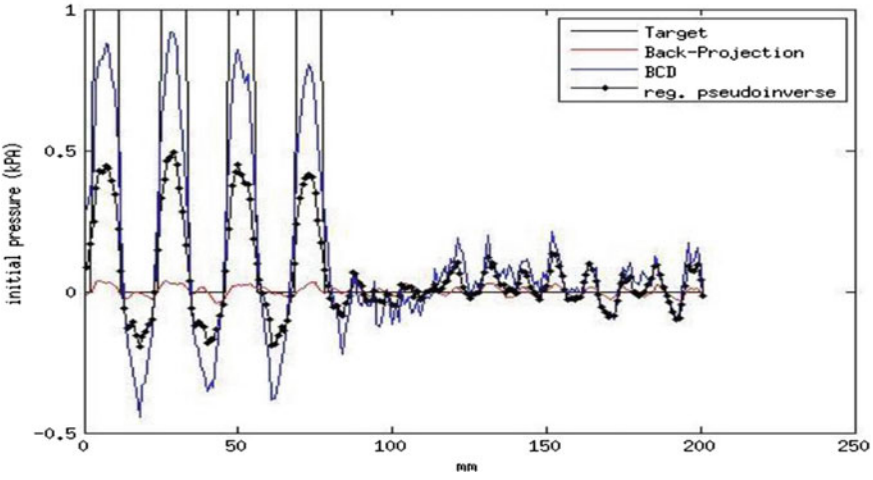

(e) Line profile for the dashed line along the target image

Fig. 4 Reconstructed photoacoustic image of a numerical Derenzo phantom as the imaging domain with an initial pressure rise of 1 kPa. **a** Target image, **b** back-projection (BP) reconstruction, **c** BCD scheme reconstruction, **d** reconstruction using regularized direct pseudo inverse computation and finally **e** the graph represents the line profile for the dashed line along the target image

(a) Target

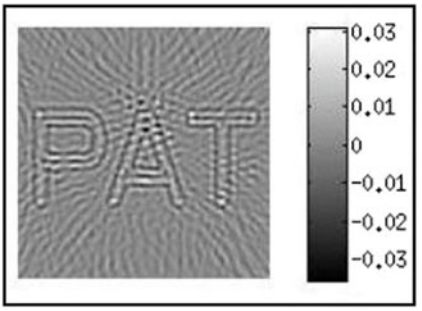

(b) Back projection

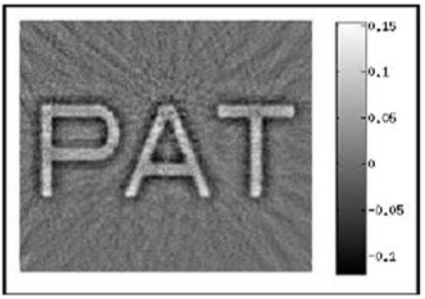

(c) BCD Reconstruction scheme

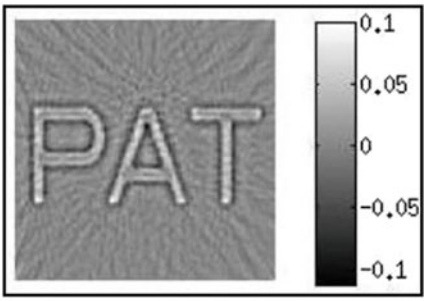

(d) Direct regularized Pseudo Inverse computation

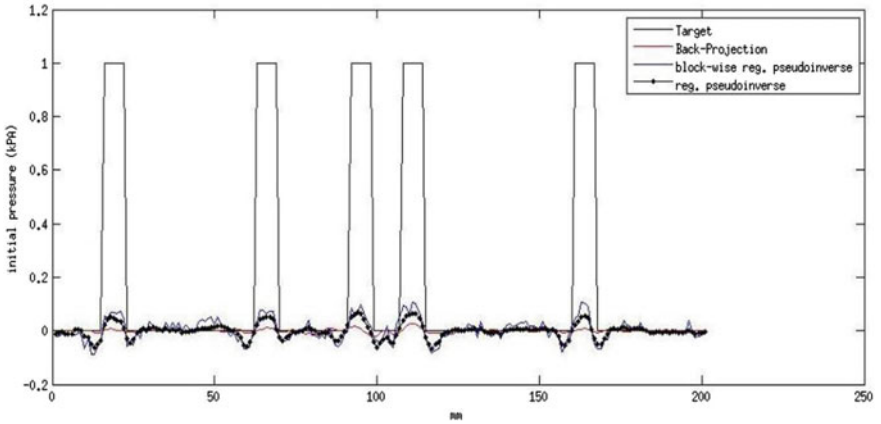

(e) Line profile for the dashed line along the target image

Fig. 5 Reconstructed photoacoustic image of a numerical PAT phantom as the imaging domain with an initial pressure rise of 1 kPa. **a** Target image, **b** back-projection (BP) reconstruction, **c** BCD scheme reconstruction, **d** reconstruction using regularized direct pseudo inverse computation and finally **e** the graph represents the line profile for the dashed line along the target image

Table 1 Computational time recorded for all pseudo inverse computation methods presented

Method for pseudoinverse computation	Time (s)
Direct methods	639
BCD (4 blocks)	213
BCD (9 blocks)	125

Table 2 Computational time simulated for various reconstruction techniques

Method	Time (s)
1. $x = A^{\mathrm{T}}b$	0.4
2. $x = A_{\mathrm{reg}}^{+}b$	0.4
3. $x_i = A_i^{+}b$	4
4. $x_i = A_i^{+}(b - A_{-i}x_i)$	21

Table 2 the computation time for image reconstruction through various methods.

5 Conclusion

In this work, a method based on block coordinate descent is proposed for image reconstruction in photoacoustic tomography. It is concluded that pseudoinverse computation takes much lesser time by dividing it into uniform size blocks. When the 201 × 201 grid size is divided into four blocks, this computation took one-third of the time when computed directly. A division into nine blocks took almost one-fifth times. The image reconstruction through BCD scheme gives quantitatively better result. This could be observed from the reconstructed images that BCD approach has better quantitativeness than back-projection and direct pseudoinverse computation approach.

The choice of regularization parameter was taken as 0.018. This value was chosen after observing the effects of on image reconstruction. It was observed that however, a lesser value of gives a lesser relative error in image reconstruction but the image quality has to be compromised.

One iteration of BCD takes approximately 21 s. It was observed that more iterations of BCD scheme improves image quality and has the scope of further improving quantitativeness. However, more number of iterations takes more time to reconstruct an image which is not so favorable.

Reference

1. Wang, L.V. (ed.): Photoacoustic Imaging and Spectroscopy. CRC, London (2009)
2. Wang, L.V.: Tutorial on photoacoustic microscopy and computed tomography. IEEE J. Sel. Top. Quantum Electron. **141**, 171179 (2008)
3. Wang, L.V.: Prospects of photoacoustic tomography. Med. Phys. **35**, 12 (2008)

4. Oraevsky, A.A., Wang, L.V.: Photons Plus Ultrasound: Imaging and Sensing, vol. 643, SPIE, Bellingham (2007)
5. Zhang, H.F., Maslov, K., Stoica, G., Wang, L.H.V.: Functional photoacoustic microscopy for high- resolution and noninvasive in vivo imaging. Nat. Biotechnol. **247**, 848–851 (2006)
6. Treeb, B.E., Cox, B.T.: K-wave: MATLAB toolbox for the simulation and reconstruction of photoacoustic wave fields. J. Biomed. Opt. **15**(2), 021314 (2010)
7. Bagchi, S., Roy, D., Vasu, R.M.: Forward problem solution in photoacoustic tomography by discontinuous Galerkin method. J. Opt. Soc. Am. (2011)
8. Xu, M.H., Wang, L.V.: Universal back-projection algorithm for photoacoustic computed tomography. Phys. Rev. E755 (2005)
9. Zhdanov, M.S.: Geophysical Inverse Theory and Regularization Problems, 1st edn. Elsevier Science BV (2002)
10. Zhiwei (Tony) Q., Scheinberg, K., Goldfarb, D.: Efficient Block-Coordinate Descent Algorithms for the Group Lasso
11. Shaw C.B.: LSQR—based automated optimal regularization parameter selection fo photoacoustic tomography, SE-360 project, Apr 2013